Composites Part B 256 (2023) 110640

Contents lists available at ScienceDirect

Composites Part B

journal homepage: www.elsevier.com/locate/compositesb

Fiber-reinforced liquid crystalline elastomer composite actuators with multi-stimulus response properties and multi-directional morphing capabilities

Yuliang Xia [a,1], Tong Mu [a,1], Yang He [a], Yanju Liu [b,**], Jinsong Leng [a,*]

[a] Centre for Composite Materials and Structures, Harbin Institute of Technology (HIT), No.2 Yikuang Street, P.O. Box 3011, Harbin, 150080, People's Republic of China
[b] Department of Astronautical Science and Mechanics, Harbin Institute of Technology (HIT), P.O. Box 301, No. 92 West Dazhi Street, Harbin, 150001, People's Republic of China

ARTICLE INFO

Handling Editor: Prof. Joong Lee

Keywords:
Liquid crystalline elastomer composite
Smart material structure
Thiol-acrylate reaction

ABSTRACT

Liquid crystalline elastomers (LCEs) are promising materials for soft actuations. LCE composites (LCECs), via the inclusion of fillers into LCEs, bring diverse functionalities and stimuli-responsive capabilities. It is still a challenge to improve the mechanical properties of LCEC and ensure that the material can perform reversible transformations. Here we present a cost-effective LCEC design and fabrication method by dispersing continuous carbon fibers and carbon nanotubes into LCEs, forming a new type of LCEC actuator. We found that through adjusting the angle (such as 45° and 90°) between the carbon fiber and the stretching axis of LCEC matrix, complex deformable geometries can be easily achieved including bending and twisting structures with enhanced storage modulus (400.9 MPa at 25 °C). Furthermore, the LCEC actuators could be driven by various stimuli including heat (120 °C), light (800 mW cm^{-2}), and electricity (2.0 V). As a result, our new LCEC actuator outperforms other LCE actuators by having the largest number of morphing geometries and stimulus-responsive modes. Our LCEC design and manufacturing strategy represents a promising general methodology that can be easily extended to other continuous fibers (such as glass fiber, aramid fiber, etc.) filled LCECs, bringing even rich shape-changing capabilities that are needed for soft robots and beyond.

1. Introduction

Soft actuators are one of the most vital components of soft robot systems [1–3]. Compared to conventional rigid actuators, soft actuators are pliable, deformable, and have a high degree of flexibility, and thus can better adapt to complex and unknown environments [4–7]. This makes them exceptionally advantageous for physical interactions with fragile objects or living beings. To date, soft stimulus-responsive materials like shape memory polymers [8–12], electroactive polymers [13,14], liquid crystalline elastomers (LCEs) [15–18], and hydrogels [19–21] have been utilized as actuators to provide a variety of mechanical actuations and deformations.

LCEs have been one of the most appealing stimulus-responsive soft materials [15,22–24]. The shape morphing of LCEs is reversible when they are exposed to specific external stimuli in many environments (e.g., indoor environment, water environment, vacuum environment) [25–27], which cannot be achieved easily by virtue of other stimulus-responsive materials. For the sake of developing LCEs with higher actuation efficiency, higher physical strength, and larger thermoconductivity and electroconductivity or designing LCEs that are capable of responding to several stimuli, various methods have been proposed by the integration of fillers into LCE matrices [2,28,43]. Due to the features of fillers, LCE composites (LCECs) can respond to heat [2,29], irradiation [30–37], magnetism [38], etc. Those LCECs are prospective materials which can provide novel functions with brilliant actuation properties via synergic effects between LCE matrices and fillers.

At present, the designing of LCECs is primarily based on reinforcing existent properties or endowing new attributes and functions via filler embedment, which is not desirable to improve the mechanic properties

* Corresponding author.
** Corresponding author.
E-mail addresses: yj_liu@hit.edu.cn (Y. Liu), lengjs@hit.edu.cn (J. Leng).
[1] These authors contributed equally to this work.

https://doi.org/10.1016/j.compositesb.2023.110640
Received 15 November 2022; Received in revised form 9 February 2023; Accepted 20 February 2023
Available online 28 February 2023
1359-8368/

of these materials [28]. There are substantial studies on LCECs based on heat and light stimulus responses [2,29,32,37]. Nevertheless, it's still difficult to prepare conductive LCEC actuators. Conductive filler-incorporated LCECs are not electroconductive because of unsatisfactory dispersity, but high electroconductivity is vital for soft robots and soft electronic devices [15,22]. Furthermore, to create intricate and monolithic 3D geometries from a 2D sheet, it's pivotal to spatially control the 2D liquid crystal director at the micro scale via a mold or mask. Thus, to create diverse shapes, novel structures of liquid crystal director molds have to be developed for LCE films [26,39].

Herein, we proposed a stress-assisted LCE/carbon fiber composite (LCEC) fabrication procedure to develop various 3D structures that could be driven by heat, light, and electricity. For the first time, carbon fibers are utilized to enhance the mechanical property, produce the electricity stimuli, and determine the 3D structures of LCEC actuators. We started with manufacturing LCEC-based 3D actuators by changing the stretching path of the LCE membrane and the angles of the continuous carbon fiber axes (0°, 45°, and 90°) without the need of a complex director mold. During the programming procedure, monodomain LCECs acquired were fixed into predetermined three-dimensional geometries (e.g., bend and twist) due to LCEs' high elasticity after UV curing. Finally, a retractable ribbon, a soft gripper, a inchworm-like robot, and their assemblies that could be driven by multiple stimuli including heat (120 °C), light (800 mW cm^{-2}), and electricity (voltage = 2.0 V) were fabricated. The results and prototyes presented in this paper show that the proposed method is quite prospective for soft robotics in fragile or complicated environments, due to their flexible and adaptive morphing properties.

2. Experimental methods

2.1. Materials

Pentaerythritol tetra(3-mercaptopropionate) (PETMP, a thiol crosslinker, Sigma-Aldrich Corp.), RM82 (a LC monomer, HCCH Company), 1-[4-(2-Hydroxyethoxy)phenyl]-2-hydroxy-2-methyl-1-propan-1-one (HHMP, a photocuring agent, Sigma-Aldrich Corp.), butylhydroxytoluene (BHT, an antioxidant, Sigma-Aldrich Corp.), 1,2-Bis(2-mercaptoethoxy)ethane (EDDET, a thiol chain extender, Sigma-Aldrich Corp.), Triethylamine (a catalyst, Sigma-Aldrich), carbon nanotubes (Shanghai Aladdin Reagent Corp.), silicone glue (PH8860, Pinheng company), and continuous carbon nanofiber filament(Toray T300B-1000-50B) comprising 1000 carbon fibers with diameter about 7 μm were directly applied without further treatment.

2.2. Preparation of polydomain LCECs

RM82 (2.01g), pentaerythritol tetrakis (3-mercaptopropionate) (0.144 g), thiol chain extender EDDET (0.431g), antioxidant BHT (0.04g, weight percentage 1.5%), carbon nanotubes (0.0026g, weight percentage 0.1%) and photo initiator HHMP (0.052g, weight percentage 2%) were blended in a 50 ml beaker, and heated at 85 °C for 30 min, which formed a molten solution. The molar ratio of the thiol functional groups between EDDET and PETMP was 4:1. The catalysis TEA (0.032g) was then introduced to the solution. We mixed the solution for 30 s and poured it in a Teflon mold with a groove thickness of 1 mm, with unidirectional continuous carbon fibers arranged above at an interval of 1 mm. Polydomain LCECs were obtained after the cooling of the sample at ambient temperature overnight and the demolding process.

2.3. Preparation of monodomain LCECs film

By stretching the polydomain LCECs at 180% strain after a 10-min UV irradiation (50 mW cm^{-2}), we prepared the monodomain LCECs with homogeneous orientation. LCEC actuators exhibited complex and programmable shapes through the adjustment of the angle α between the tensile direction of the sample and the carbon fiber axis. After the removal of the clamps on both ends of the sample during curing, when α = 45°, the sample became a twist shape after UV curing, when α = 90°, the sample presented a bend shape after the curing by UV light.

2.4. Characterization

Absorbance spectra: By generating the Fourier transform infrared spectroscopy (FTIR), we investigated the specimens via a PerkinElmer Spectrum Two FTIR spectrometry detector. The spectra have been gained in an ambient environment with the 2 cm^{-1} resolution at 40 scans under the total reflectance method. in terms of respective characterization.

2D-wide angle XRD (2D_WAXD) characterization: The anisotropic alignment of the sample was characterized through the 2D-WAXD experiment via a Xeuss 2.0 diffractometer with a Pilatus 300K detector under the Line Eraser mode. The monodomain sample was tested at 25 °C and 120 °C, respectively.

Dynamic mechanical analysis (DMA): The DMA assays were completed under a tension mode via a DMA Q800 from TA Instruments, USA. The mechanic properties have been examined under a multi-strain mode at −50 °C–200 °C, with a 5.0 °C/min heating velocity and 1 Hz frequency. The maximum elongation strain was examined under the force-control mode at room temperature. The reversible actuation strain was examined, ranging from 25 °C to 200 °C. The size of samples subjected to DMA assays was 30.0 × 8 × 0.2 mm^3.

Differential scanning calorimeter (DSC) test: The DSC measuring was conducted in nitrogen with a DSC 1 STAR System (Mettler-Toledo). Samples have been cut into little pieces and set in aluminum pans. To discover the transition temperature of the sample, the experiment was carried out from −30 °C to 200 °C, and cooling back to −30 °C at 10 °C/min during each cycle.

Thermogravimetric analysis (TGA): The actual fiber content and thermal stability were examined via TGA through a TGA/DSC 1 STAR System, with samples heated from 25 °C to 1000 °C with a heating rate of 10 °C/min under the inert environment.

Actuation and Thermal Performance of LCECS: The thermo actuation of the LCECs was performed using a hot air gun (KaiLiwei Co.). Monodomain twist and bend actuators were localized and heated from the ambient temperature to 120 °C in 15 s to illustrate the different transforming processes.

The light actuation of the LCECs was performed using a spectrometer under a full spectrum mode. The hook-like samples showed reversible deformation due to the day light irradiation at an intensity of 800 mW cm^{-2} (Beijing Newbit Technology Co., Ltd.) for 21 s. The inchworm-shaped sample was placed on a platform with a slope of 5°, and subjected to repeated cycles of illumination for 15 s and cooling for 60 s, to stimulate the sample to realize the diagonal movement down the platform.

The electricity actuation of the LCECs was performed using ITECH DC, Source Meter at 2.0V. The magnitude of the current was regulated by controlling the voltage across the carbon fiber. Subsequently, the reversible deformation of the sample was stimulated through electric heating.

The infrared thermographic test was completed with an infrared camera. The JENOPTIK camera (InfraTec) was utilized to explore the temperature of different samples (e.g., the temperature distribution during the reversible transformation).

3. Results and discussion

We designed different deformable actuators containing stimuli-responsive LCE matrix and carbon fiber as schematically illustrated in Fig. 1. The diacrylate RM82, PETMP, EDDET, BHT , and HHMP were chosen, separately, as the LC monomer, thiol crosslinker, thiol extender, antioxidant, and photoinitiator for the synthesis of the polydomain

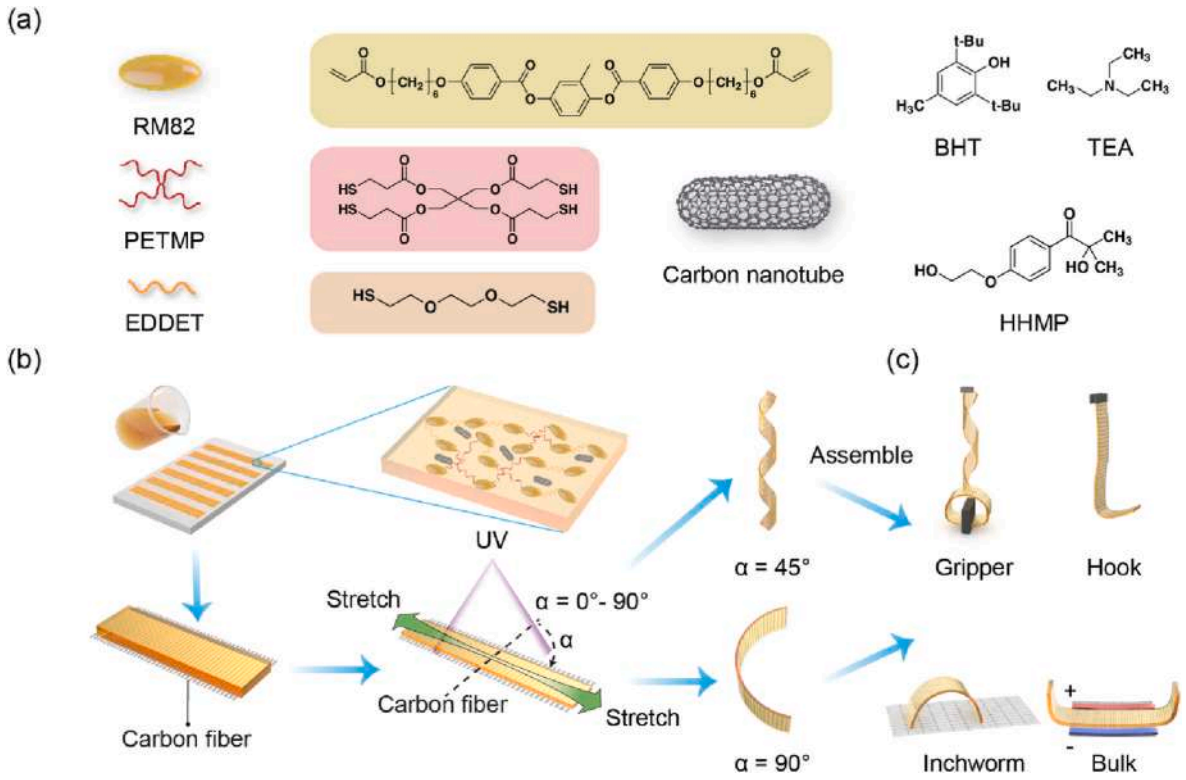

Fig. 1. Schematic of the fabrication process of LCEC actuators. (a) Chemical structure of monomers for preparing LCEC actuators; (b) Processes of fabricating LCEC actuators with different stretching angle between LCE matrix and carbon fiber. The angle of the sample is measured prior to stretching. When $\alpha = 0^\circ$ or $\alpha = 90^\circ$, there is no change in the angle of the sample after stretching. When $\alpha = 45^\circ$, the final angle will present further rotation into 30 ° after stretching; (c) Scheme of the different assemblies of LCEC actuators.

LCEC sample. Equal molar amounts of acrylate functional groups and thiol functional groups were utilized in the reaction. The thiol click chemistry reaction was catalyzed using TEA as a basic catalyst, and LCE precursors were prepared with certain flexibility (Fig. 1a).

The mechanical programming of the LCEC actuators in this study consisted of three steps (Fig. 1b). First, polydomain LCECs were synthesized by straightly casting the molten of the aforementioned reactants in Teflon molds, with continuous carbon fiber aligned parallel at a spacing of 1 mm. The synthesis details were presented in the Experimental Section. During the aforementioned process, the molten was transformed into the polydomain LCECs after cooling overnight through a phase transition. This process didn't require the intervention of other solvents such as chloroform. The polydomain LCECs formed in the aforesaid process exhibited certain mechanical strength, which could sufficiently allow them to be smoothly released from the mold. Antioxidants decreased the degree of crosslinking of the prepolymer during the process, thus making it easier to be stretched into the monodomain state.

Second, uniaxially-orientated (monodomain) LCECs were acquired via stretching polydomain LCECs, in which randomly distributed LCs were oriented into 1 orientation. The above orientation of LCs could be the prerequisite for the heat actuation behaviors of LCECs. As per the tensile test of LCECs, a strain of 180% was chosen during the stretching process, since it was significantly smaller than the breaking strain and it was sufficient to transform the LCECs from the polydomain phase to the monodomain phase. As indicated by the results of the preliminary trials, the chosen 180% strain caused monodomain LCECs with a uniformed orientation. The stretching direction of the LCE and the axis direction of the carbon fiber were set as the α angle. The LCECs were stretched with different α angles (e.g., $\alpha = 0^\circ$, 45°, and 90°). When $\alpha = 0^\circ$, the strength of the carbon fiber along the axis direction was too large to be broken, thus causing the LCE to lose its flexibility in the axial direction and making it unable to be stretched to form the monodomain state. Thus, the main research object of this experiment was to obtain the LCE composite materials with α angle of 45° and 90°.

At the last step, the monodomain programmed stretched shape was fixed through the UV triggered cross-linking. During this step, the photoinitiator enabled the remained uncrosslinked functional groups in the polydomain LCE synthesis step to react further under the radiation of ultraviolet light to form a further cross-linked grid structure. Depending on the α angle, as the external stress has been removed, the ultimate shapes of the monodomain LCECs transformed to bend ($\alpha = 90^\circ$) and twist ($\alpha = 45^\circ$).

The uniqueness of this method is that the LCECs after UV fixation would present different morphologies. When $\alpha = 45^\circ$, the sample was twisted into a spiral state along the direction of the continuous carbon fiber axis. The sample was bent into a bend shape vertical to the direction of the continuous carbon fiber axis as $\alpha = 90^\circ$. The sample was not observed with any specific bend orientation when the carbon fiber was not used. Both of them exhibited the characteristics of reversible deformation during heating and cooling cycles. As revealed by the results, it would be feasible to design LCECs with different deformation modes by simply changing the angles of carbon fibers and the stretching orientation of the LCE matrix (Fig. 1c). The detail comparison with other literature could be found in Table 1.

In order to optimize the low-temperature grasping capabilities of LCEC with higher stiffness and energy efficiency, we designed an initial bending structure with fiber on the inner surface. During training, the material is given a initial curvature. This allows LCEC to be straightened in a heated state and close to the object for grasping, and then cooled down, enabling LCEC to adaptively grasp the object.

Table 1
Summary of the stimulus methods and geometries of LCECs in the literature.

Incorporation materials	Stimulus methods			Geometries				References
	Heat	Light	Electric	Bend	Twist	Gripper	Inchworm	
Carbon nanotube	✓	✓	×	✓	×	×	×	[33]
Carbon nanotube	✓	✓	×	✓	✓	×	×	[29]
Carbon black	✓	×	✓	✓	×	✓	✓	[7]
Gold nanorod	✓	✓	×	✓	×	×	×	[37]
Gold nanoparticle	✓	✓	×	✓	×	×	×	[26]
Liquid metal	✓	✓	×	✓	×	×	✓	[31]
N/A	✓	×	×	✓	✓	✓	×	[39]
Carbon nanotube, carbon fiber	✓	✓	✓	✓	✓	✓	✓	This work

3.1. Spectra analysis

To investigate the chemical reaction process during polymer synthesis, spectroscopic analyses were carried out to characterize the Michael-addition reaction. Different functional groups in the polymer were characterized through FT-IR analysis. The result indicated that the thiol functional group peaking at 2568 cm^{-1} in polydomain LCEs vanished. The acrylate functional group (peak at 810 cm^{-1}) was maintained posterior to the thiol-acrylate reactive process (Fig. 2), which revealed that the thiol groups and certain acrylate groups were still in the first step and reacted during the UV curing process. The above feature was found to be consistent with the scheme designed in our polymer synthesis route [40].

The order of liquid crystals changed at different temperatures, which was discovered by performing 2D-WAXD experiments on the samples at 25 °C and 120 °C. The 2D-WAXD experiments could be an effective method to observe from the Debye ring and identify whether the sample was oriented at the microscopic level. The monodomain LCEs showed a uniaxial orientation along the direction of mechanic stretching through the characterization with 2D-WAXD features (Fig. 3a). In particular, the reflection at 2θ = 19.81°was significant, representing a d-spacing of nearly 4.47 Å, which demonstrated a pair of nematic arcs. When the temperature rose to 120°, the temperature was higher than the nematic-isotropic transition temperature (T_{NI}) of the sample, so the LC lost its orientation, and 2D-WAXD showed a regular isotropic ring at 2θ = 18.04°, demonstrating a d-spacing about 4.91 Å (Fig. 3b). The azimuthal intensity under 25 °C and 120 °C has been demonstrated in Fig. 3c, which demonstrated the orientation change of LC at different temperatures [41,42]. The microstructure of LCECs has been thoroughly characterized and discussed in Supplemental text 1 and Fig. S1.

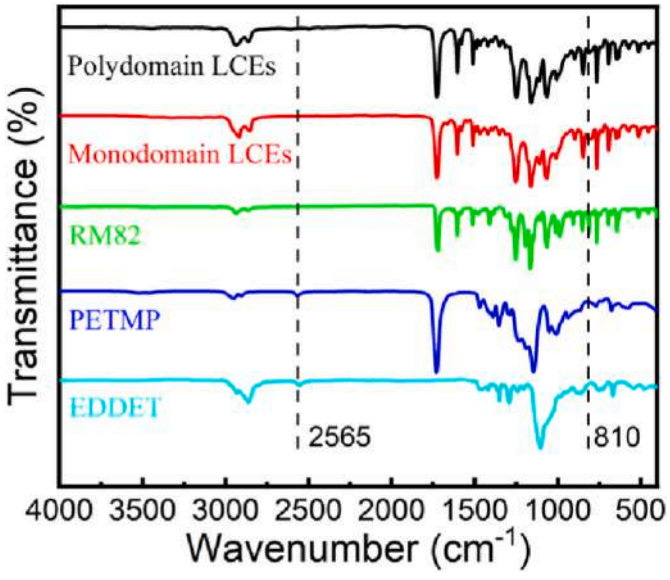

Fig. 2. FTIR of LCEs synthesized by thiol-acrylate reaction.

3.2. Thermo mechanical properties of LCECs

To quantify the improvement in LCECs, thermo mechanical properties of LCEC and LCE is tested. DMA tests were first performed on samples with different α angles from −50 °C to 200 °C. There was a significant difference in modulus between the polydomain LCE and the UV crosslinked monodomain LCE (Fig. 4a). In this interval, the crosslinked monodomain LCEs presented a high modulus of 1400 MPa compared with the polydomain LCEs (400 MPa). It was further explained that during the polymer synthesis step, the base catalyst failed to realize the thorough reaction of the reactants. As the temperature rose, the modulus of the samples tended to decrease. The elasticity of the sample decreased since the temperature was already above the T_g of the polymeric material. With the temperature rise, the samples with different α angles exhibited different moduli simultaneously. The modulus of the LCECs sample with α = 0° was about 400.9 MPa at 25 °C and maintained over 60 MPa across the DMA characterization, which thus evidenced that the carbon fiber was well compounded with the material matrix. Compared with the monodomain LCE without carbon fibers, the modulus of the LCECs with α = 90° did not significantly increase, which was about 5.1 MPa at 25 °C. The modulus of LCECs with α = 45° increased, reaching 10.2 MPa at 25 °C (Fig. 4b). The loss factor (Fig. 4c) can be used to represent the transition temperature and mechanical properties of the composite. The first peak of the loss factor corresponds to the glass transition temperature (Tg) of the composite. The T_g of polydomain LCE and monodomain LCE was determined to be −12.9 °C and −10.2 °C, respectively. Additionally, the T_g of LCECs with "α = 90°, α = 45°, α = 0°" was observed to be −15.1 °C, 6.2 °C, 12.5 °C respectively. This increase in Tg suggests that the bond between the carbon fiber and the matrix has a greater effect on the composite, requiring it to absorb more energy for the polymer chain segments to slide. The width of the peak can be used to measure the interfacial bonding strength between the fiber and the resin matrix, as well as the energy required for the chain segment to start moving. It can be seen that LCECs with "α = 0°" and "α = 45°" have wider peak widths than polydomain LCE, monodomain LCE and LCECs with "α = 90°", suggesting that the interface binding strength of the two is strong and the chain segment motion requires more energy [44,45]. The tensile test was performed at ambient temperature. When α = 45°, the sample displayed a strain up to 350.1% of 2.7 MPa without broken (Fig. 4d). The monodomain LCE sample demonstrated a stress of 1.7 MPa under the same strain. When α = 0°, the strength of the carbon fiber was highly different from that of the LCE matrix, thus resulting in the uneven fracture of the sample.

To further verify the thermal properties of the LCECs, we characterized the thermal characteristics of monodomain LCECs, which could be important for achieving 3D shape variations. The deformation mechanism of LCEs originates from the phase transition of liquid crystal (LC) molecules across the T_{NI} [46,47]. The T_{NI} was identified via differential scanning calorimetry (DSC). The samples all exhibited T_{NI}, where the polydomain LCE owns T_{NI} at 83.3 °C, the monodomain LCE

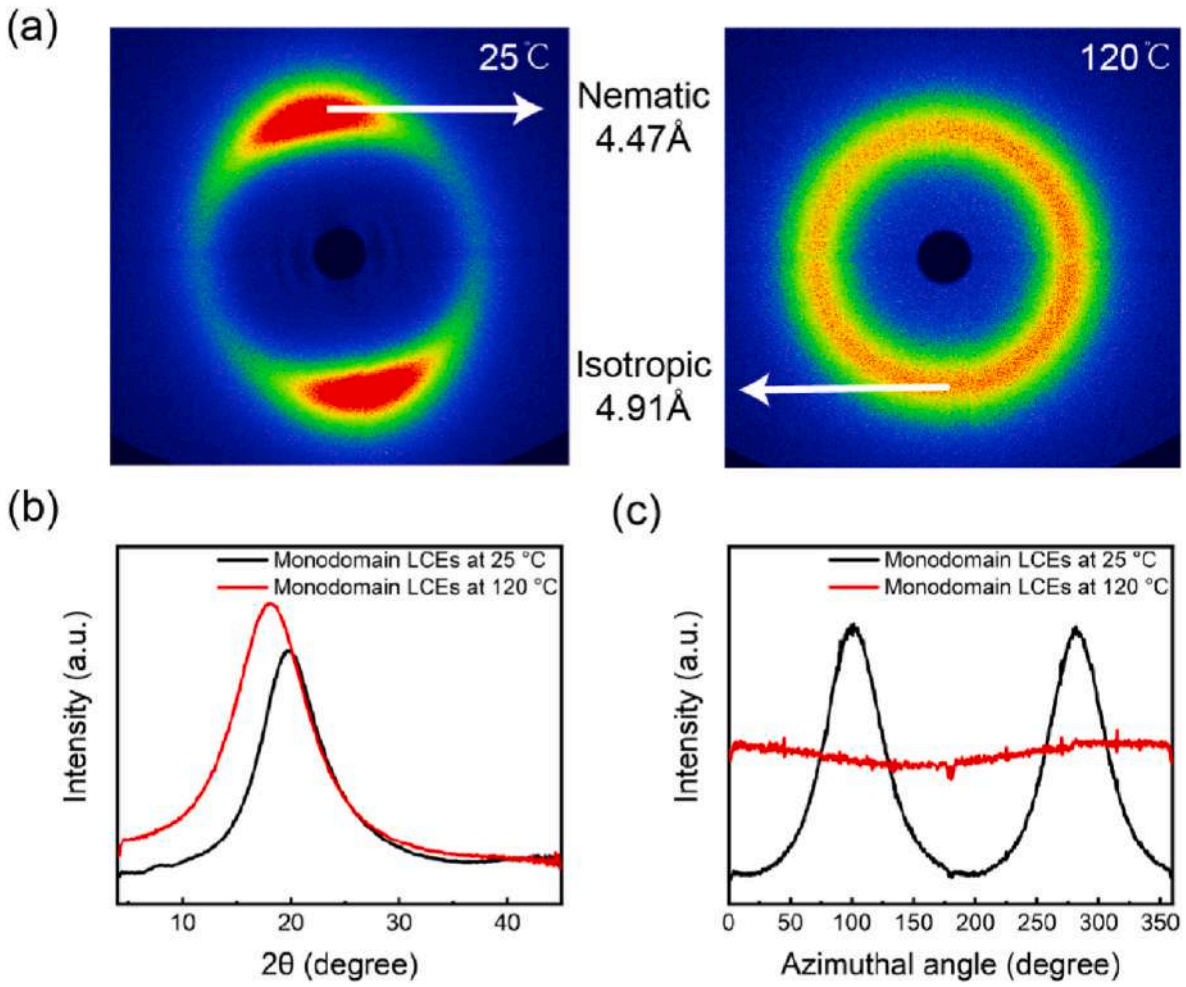

Fig. 3. 2D-WAXD characterizations of LCE samples under different temperature (a) 2D-WAXD patterns of LCECs under 25 °C (left) and 120 °C (right) (b) WARD curves of monodomain LCEs. (b) The peaks round$2\theta = 19.81^{\circ}$ a and $2\theta = 18.04^{\circ}$corresponding to nematic phase and isotropy phase. According to the equation $\lambda = 2d \sin\theta$ ($\lambda = 1.54$ Å), the d-spacing of nematic phase and isotropic phase are 4.47 Åand 4.91 Å (c) Azimuthal intensity scan of the X-ray diffraction patterns from monodomain LCEs under different temperature.

owns T_{NI} at 91.6 °C, and the LCECs owns T_{NI} at 92.8 °C (Fig. 5a). The polydomain LCE exhibits T_{NI} as well, indicating that the material undergoes a phase transition. However, this phase transition does not guarantee the reversible deformation capability of the LCE. To ensure reversible deformation at room temperature, the mesogen unit in the LCE must be pre-stretched and fixed. Additionally, the T_{NI} peak of monodomain LCE and LCECs are not obvious due to the sample history. Similar phenomenon has been reported in the previous research [26]. The degradation temperature of LCECs was 351.1 °C, which was remarkably higher in contrast to the T_{NI}, ensuring the steady heat actuation behaviors of LCEC actuators (Fig. 5b). On the premise that the rigidity of the polymer was ensured, thermodynamic cycling experiments based on LCECs were performed to test the recoverable deformation rate of LCEC composites at high and low temperatures. The temperature range applied was 25–200 °C, a common operation temperature range for LCEs, and the T_{NI} was also included. The results showed that LCECs exhibited a good reversible deformation ability, and it obtained a reversible elongation of 57.1% at a stress of 0.2 MPa (Fig. 6).

3.3. Thermo driven LCECs

Given the thermomechanical features of the synthesized LCECs, we proposed a programming procedure that could be feasible for preparing programmable LCEC actuators with multiple deformation modes. In the conventional preparation method, the shape of LCEs is determined by the post-setting. In the process of post-setting, the mold and external force factors should be used to convert the LCEs into a predetermined fixed shape with UV curing. In this way, the transformation of LCEs into different 3D shapes requires different molds and additional external force, which thus increases the complexity of the fabrication. The experiments indicated that by introducing continuous carbon fibers into LCE, LCECs could be shaped into different 3D structures simply by stretching the LCE matrix with photocuring, which thus eliminated the need for additional molds and external forces. In our experiments, 3D structures could be produced, which was reliant on the angle between the carbon fiber axis and the stretching direction. Here, we obtained two types of LCECs with two typical shapes, such as bend and twist, by setting $\alpha = 90^{\circ}$ and $\alpha = 45^{\circ}$. Both structures exhibited satisfactory thermally-driven reversible deformation behavior, which could serve as an actuator in different circumstances.

According to the results of the thermodynamic cycle, we firstly demonstrated the deformation of samples with different α angles at ambient temperature and 120 °C through direct heating (Fig. 7a and b). Both the twist and bend samples displayed stable reversible deformation, which resulted in significant thermal shrinkage in about 15 s and cold extension characteristics in 20 s (Supporting information, Movie S1 and Movie S2). The above result indicated that it could be feasible to fabricate LCECs with complex multifunctional modes by combining different LCEC actuators. By combining the end of the actuator with α =

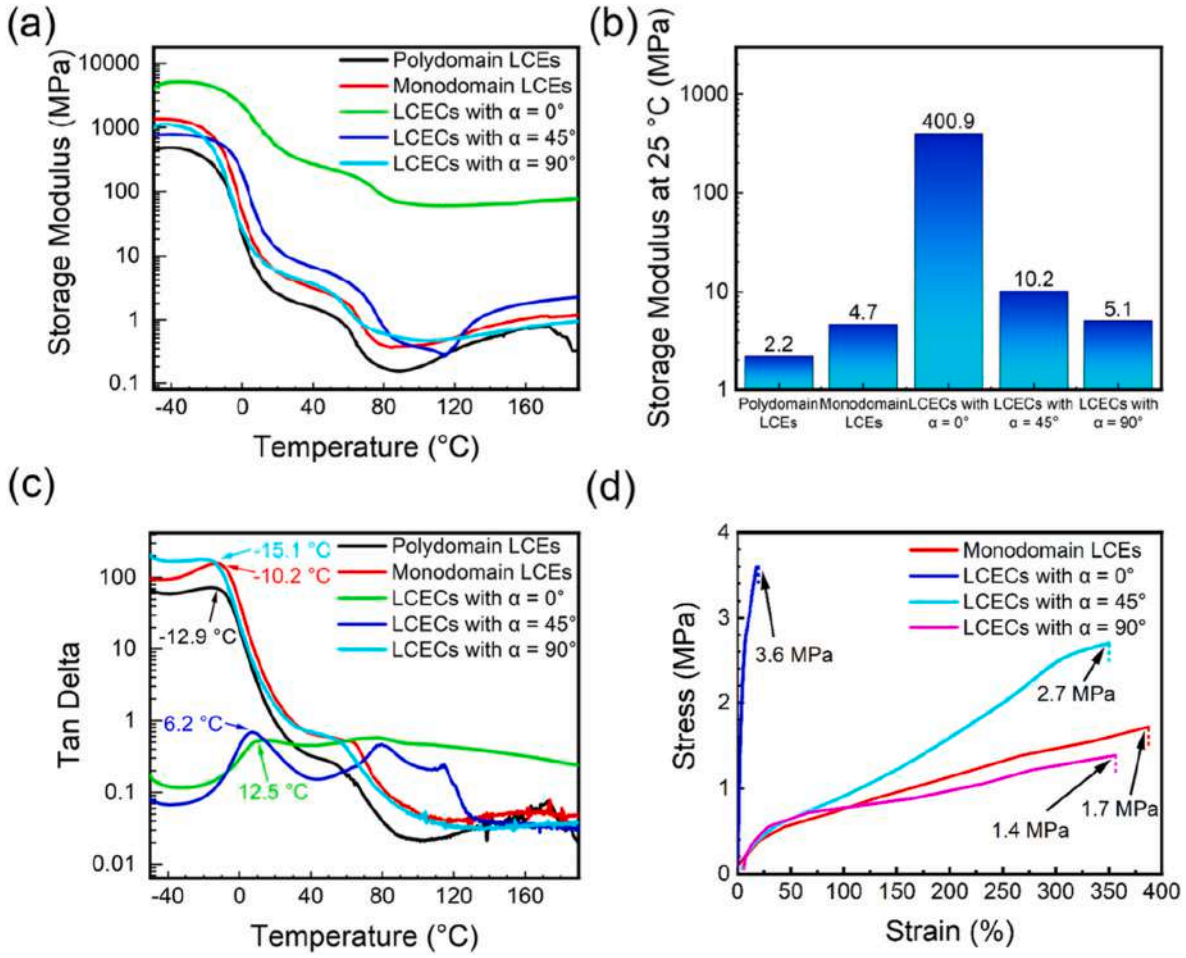

Fig. 4. DMA curves of LCEC samples with various fiber orientations (a)The storage modulus of different LCEC samples from −50 °C to 200 °C; (b) The storage modulus of different LCEC samples at 25 °C (c) The loss factor of different LCEC samples from −50 °C to 200 °C; (d)Tensile test of the LCECs under the applied stress at 25 °C. The load direction coincident with that of the longitudinal axis of the specimen shown in Fig. 1b.

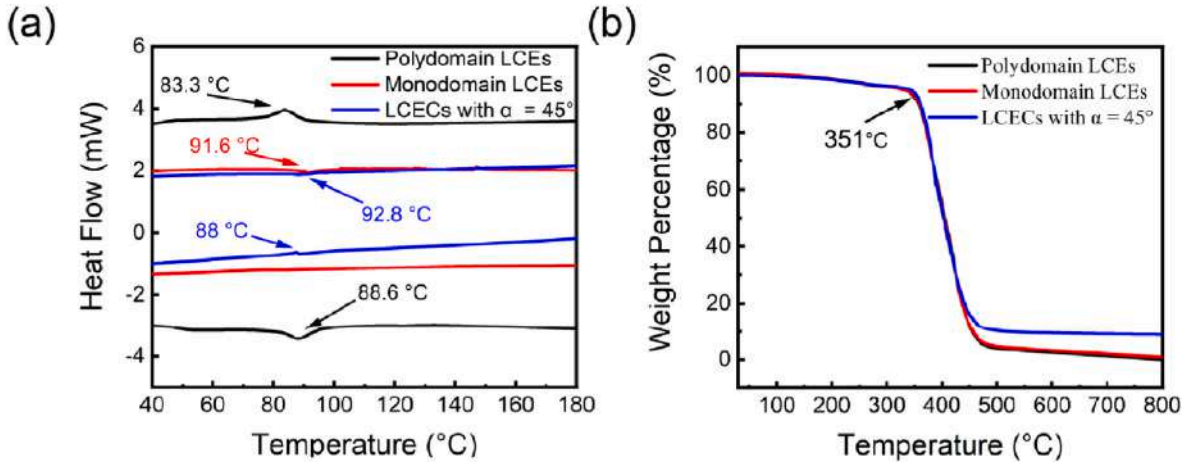

Fig. 5. (a) DSC curves of LCEC specimens in N_2 environment; (b) TGA curves of LCEC specimens in N_2 environment.

45° to the middle of the actuator with α = 90° through silicone glue, we further produced a multifunctional LCEC gripper that could be locally deformed. The silicone glue exhibits a strong adhesive force, allowing two surfaces to be joined together securely with minimal contact area, thus avoiding any impediment to the deformation of the two surfaces. (Fig. 7c). The spiral LCEC part served as the extension mechanism of the gripper to control the extension and contraction of the gripper in the vertical direction. The bend LCEC part acted as a locking mechanism for the gripper to grab and release objects. The gripper was capable of expanding, contracting, capturing and releasing foam (201 mg) by adjusting the local temperature (Movie S3).

Supplementary data related to this article can be found at https://doi.org/10.1016/j.compositesb.2023.110640.

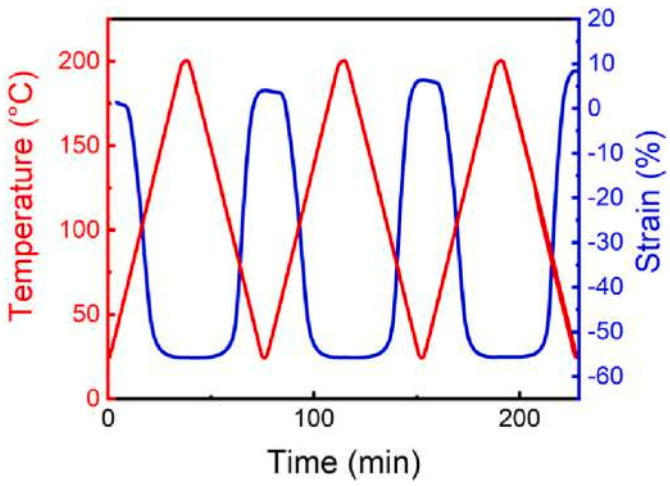

Fig. 6. Reversible thermo cycling behavior of the LCECs under 0.2 MPa from 25 °C to 200 °C. The strain is axial to the sample.

3.4. Light and electricity driven LCECs

In further experiments, the different driving modes of LCECs were widened to explore their application range. Compared with thermal drive, optical drive could be more accurately selected and controlled in practical applications. We used a full spectrum instrument with a power density of 800 mW cm^{-2} to drive the hook actuator. In the above process, carbon nanotubes played a role in absorbing light to generate heat. Fig. 8a illustrates the reversible deformation and recovery of the hook LCEC actuator driven by the spectrometer. As revealed by the infrared thermal imager, the spectrometer could heat the material to 113.4 °C within 21 s during the above process with good heat distribution and recover in 31 s (Fig. 8b). The sample returned to its original hook shape during cooling (Supporting information, Movie S4). The light-responsive hook could be repeatedly actuated for at least 30 cycles. On that basis, we further fabricated a flexible inchworm driver capable of driving the crawl process by light (Fig. 8c). The inchworm driver scaled and crawled on a flat surface by the cycle of light. As a result, the inchworm could crawl on a flat plate with an angle of 5° at 6 mm per minute (Supporting information, Movie S5).

Supplementary data related to this article can be found at https://doi.org/10.1016/j.compositesb.2023.110640.

Eventually, the electrically actuated properties of LCECs were demonstrated. In this experiment, a bend-type actuator was employed. Unlike previous actuators, the bend-type actuators applied in the electricity driving mode exposed the continuous carbon fiber on the sides. By clamping the ends of the carbon fiber, we were able to apply a voltage to it to change the temperature of the actuator. The reversible deformation characteristics of LCECs under 2.0 V were well demonstrated (Fig. 8d). The sample could be locally heated up to 110 °C under energization at 2.0 V in 14 s and recover in 16 s (Supporting information, Movie S6). Based on the above method, since the carbon fiber on the side of the driver was clamped, the driver could not exhibit a large deformation. However, the relatively small deformation behavior was sufficient to prove that the motion of the LCEC actuator could be controlled by an electrical drive. The results of the electricity-driven cycle test demonstrated that the LCECs could cycle at least 80 times under this mode. The presented study designs and constructs programmable three-dimensional LCEC actuators with improved mechanical properties and multiple functions without the need for multiple molds. The aforementioned discovery is technically vital for the research of intriguing LCECs with great application potential (e.g., the emulation of biological nerve fibers and the weaving of smart textiles).

Supplementary data related to this article can be found at https://doi.org/10.1016/j.compositesb.2023.110640.

3.5. Bending mechanism of LCEC

Upon heating of the composite material, the LCE shrinks, yet the inner side of the curved structure is arranged with fibers which is far stiffer than the LCE, thereby deformation of the inner LCE is constricted [46–53]. Consequently, the deformation of the inner side of the curved structure is smaller than that of the outer side, leading to a decrease in the curvature of the LCEC structure.

When adopting the linear section assumption, let the thickness be H. The deformation of the LCEC can be divided into two components: initial bending deformation and shrinkage deformation. The curvature of the initial bending deformation is denoted as κ_0. Because of the linearity of the beam under small deformation, the total curvature is obtained by combining the curvature of the shrinkage deformation with the initial bending deformation. Subsequently, we will calculate the curvature of the shrinkage deformation.

The shrinkage of the LCE matrix can be divided into two stages. Initially, the upper and lower layers shrink uniformly until the fibers come into contact with one another. This stage does not cause any

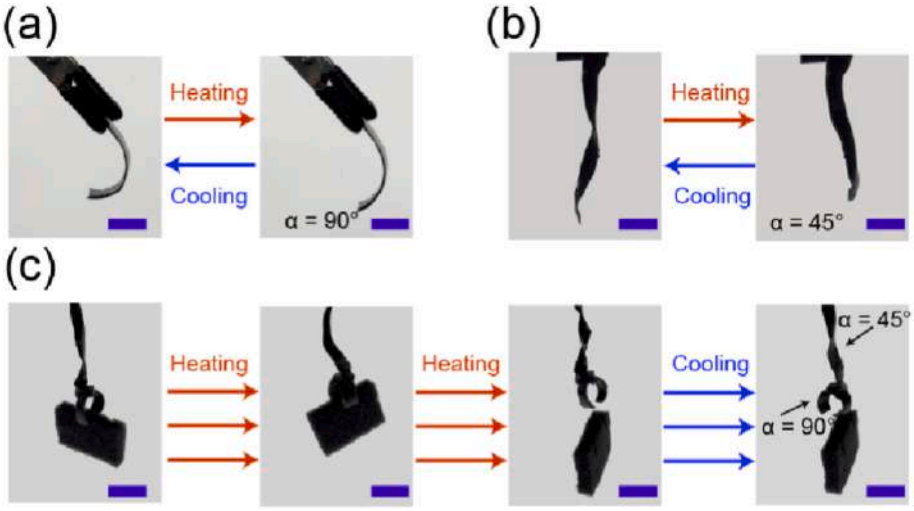

Fig. 7. Thermo behaviors of actuators with different angles (a) α = 90° and (b) α = 45° from room temperature to 120 °C (c) Illustration of foam-grabbing process with 201 mg using LCEC ribbon. Scale bar: 1 cm.

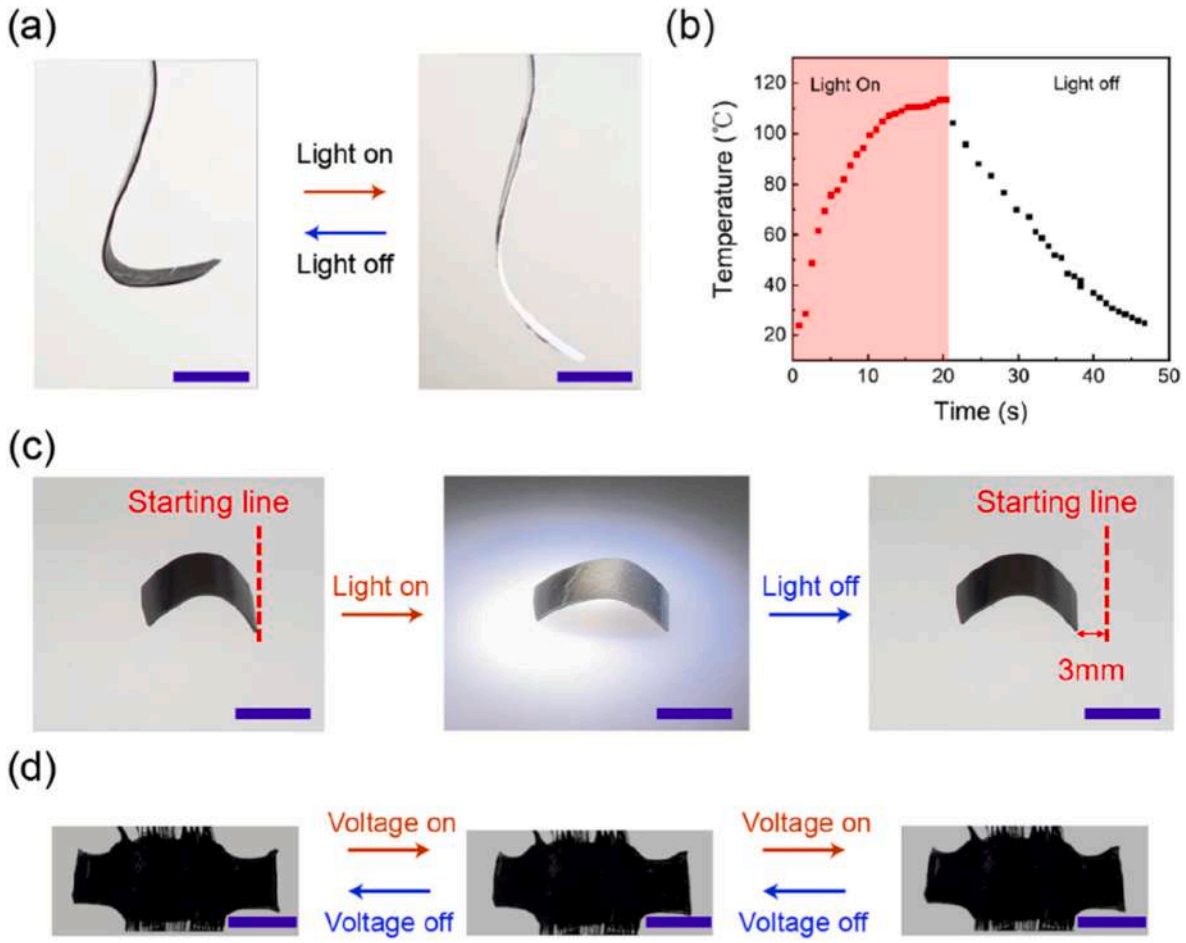

Fig. 8. (a) Light actuation of the bending motion of the hook sample; (b) temperature variation of hook sample versus time; (c) illustration of inchworm robot under light irradiation with a crawling distance of 3 mm; (d) illustration of the electricity actuation behavior of the sample under 2.0 V. Scale bar: 1 cm.

additional bending deformation. Subsequently, due to the constraints of the fibers on the inner surface, the inner surface is unable to shrink freely, while the outer surface continues to shrink, resulting in the structure bending. At this point, the inner surface where the fibers are located can be considered an incompressible membrane with no bending stiffness. Let the total shrinkage strain of LCE be ε_s, with the shrinkage strains of the first stage being ε_{s1}; then the remaining strain of the second stage is.

$$\varepsilon_{s2} = \varepsilon_s - \varepsilon_{s1}$$

Assuming that the outer surface strain in the second stage is ε_e, it can be concluded that, based on the linear section assumption, the strain energy density at a distance h from the inner surface is

$$w = \frac{1}{2}E\left(\varepsilon_{s2} - (\varepsilon_{s2} - \varepsilon_e)\frac{h}{H}\right)^2$$

According to the principle of minimum energy, we determine outer surface strain ε_e which minimizes the integral of the strain energy density along the thickness

$$\int_0^H w\, dh = \frac{EH}{6}\left(\varepsilon_e^2 + \varepsilon_e\, \varepsilon_{s2} + \varepsilon_{s2}^2\right)$$

Resulting in the outer surface strain ε_e is

$$\varepsilon_e = -\frac{1}{2}\varepsilon_{s2}$$

The strain on the inner surface is

$$\varepsilon_i = \varepsilon_{s2}$$

The radius of curvature of the inner surface shall be denoted as R, and the arc length difference between an infinitesimal central angle on the upper and lower surfaces shall be determined as

$$d\Delta L = Hd\theta = (\varepsilon_e - \varepsilon_i)R_i d\theta$$

So, the radius of curvature (ROC) of the inner surface is

$$R_i = \frac{2H}{3(-\varepsilon_{s2})}$$

Then the ROC at the central thickness is

$$R = \frac{2H}{3(-\varepsilon_{s2})} + \frac{H}{2}$$

The curvature produced by shrinkage deformation is

$$\kappa_s = \frac{6(-\varepsilon_{s2})}{4H + 3(-\varepsilon_{s2})H}$$

If the length contraction of the first stage is not taken into account, the overall curvature is

$$\overline{\kappa} = \kappa_0 + \kappa_s$$

Considering that the length of the first stage shrinks to $1 + \varepsilon_{s1}$ times than the original, the total curvature becomes

$$\overline{\kappa} = \frac{\kappa_0 + \kappa_s}{1 + \varepsilon_{s1}}$$

We can get from the experiment that

$\kappa_0 = 1.4 \times 10^2 mm^{-1}$

$\varepsilon_s = -0.3$

$H = 1mm$

$\varepsilon_{s1} = -0.2$

It can be calculated that the final heated curvature is

$\kappa = 1.75 \times 10^2$

The curvature measured in the heated state is $1.9\times 10^2 mm^{-1}$ in the experiment, and the error is 8.5%, which shows the analysis is valid.

4. Conclusion

In conclusion, a novel continuous carbon fiber incorporated LCEC actuators has been developed with an enhanced storage modulus (400.9 Mpa at 25 °C) that can be driven by heat (120 °C), light (800 mW cm^{-2}), and electricity (2.0 V) at the first time. Different shape-changing models including the bend (α = 90°) and twist (α = 45°) structures have been manufactured to design multifunctional LCEC actuators and their assemblies including retractable ribbon, soft gripper, and inchworm-like robot. The inclusion of carbon fiber has demonstrated the potential to both improve the mechanical properties and tailor the 3D deformation models of LCECs, presenting a promising fabrication approach that could be extended to other continuous fibers (glass fiber, aramid fiber, etc.) to create new LCECs. Additionally, the soft actuators and robots based on LCECs demonstrated in this study are particularly promising for soft robots operating in intricate environments.

Declaration of competing interest

The authors declare that they have no known competing financial interests or personal relationships that could have appeared to influence the work reported in this paper.

Data availability

Data will be made available on request.

Acknowledgements

This work is supported by the National Key R&D Program of China (2022YFB3805700).

Appendix A. Supplementary data

Supplementary data to this article can be found online at https://doi.org/10.1016/j.compositesb.2023.110640.

References

[1] Ilami M, Bagheri H, Ahmed R, Skowronek EO, Marvi H. Materials, actuators, and sensors for soft bioinspired robots. Adv Mater 2021;33(19):2003139.
[2] Kim H, Lee JA, Ambulo CP, Lee HB, Kim SH, Naik VV, et al. Intelligently actuating liquid crystal elastomer-carbon nanotube composites. Adv Funct Mater 2019;29 (48):1905063.
[3] Rus D, Tolley MT. Design, fabrication and control of soft robots. Nature 2015;521 (7553):467–75.
[4] Whitesides GM. Soft Robotics. Angew Chem Int Ed 2018;57(16):4258–73.
[5] Tolley MT, Shepherd RF, Mosadegh B, Galloway KC, Wehner M, Karpelson M, et al. A resilient, untethered soft robot. Soft Robot 2014;1(3):213–23.
[6] Hu W, Lum GZ, Mastrangeli M, Sitti M. Small-scale soft-bodied robot with multimodal locomotion. Nature 2018;554(7690):81–5.
[7] Wang C, Sim K, Chen J, Kim H, Rao Z, Li Y, et al. Soft ultrathin electronics innervated adaptive fully soft robots. Adv Mater 2018;30(13):1706695.
[8] Mu T, Liu L, Lan X, Liu Y, Leng J. Shape memory polymers for composites. Compos Sci Technol 2018;160:169–98.
[9] Xia Y, He Y, Zhang F, Liu Y, Leng J. A review of shape memory polymers and composites: mechanisms, materials, and applications. Adv Mater 2021;33(6): 2000713.
[10] Zhang F, Wen N, Wang L, Bai Y, Leng J. Design of 4D printed shape-changing tracheal stent and remote controlling actuation. Int J Smart Nano Mater 2021;12 (4):375–89.
[11] Gu J, Zhang X, Duan H, Wan M, Sun H. A hygro-thermo-mechanical constitutive model for shape memory polymers filled with nano-carbon powder. Int J Smart Nano Mater 2021;12(3):286–306.
[12] Margueres P, Olivier P, Mounkaila M, Sassi S, Camps T. Carbon fibres reinforced composites. Electrical impedance analysis: a gateway to smartness. Int J Smart Nano Mater 2020;11(4):417–30.
[13] Bashir M, Rajendran P. A review on electroactive polymers development for aerospace applications. J Intell Mater Syst Struct 2018;29(19):3681–95.
[14] Khan M, Li T, Hayat A, Zada A, Ali T, Uddin I, et al. A concise review on the elastomeric behavior of electroactive polymer materials. Int J Energy Res 2021;45 (10):14306–37.
[15] Wang Z, Wang Z, Zheng Y, He Q, Wang Y, Cai S. Three-dimensional printing of functionally graded liquid crystal elastomer. Sci Adv 2020;6(39):eabc0034.
[16] Zhang Y, Wang Z, Yang Y, Chen Q, Qian X, Wu Y, et al. Seamless multimaterial 3D liquid-crystalline elastomer actuators for next-generation entirely soft robots. Sci Adv 2020;6(9):eaay8606.
[17] Ware Taylor H, McConney Michael E, Wie Jeong J, Tondiglia Vincent P, White Timothy J. Voxelated liquid crystal elastomers. Science 2015;347(6225):982–4.
[18] White TJ, Broer DJ. Programmable and adaptive mechanics with liquid crystal polymer networks and elastomers. Nat Mater 2015;14(11):1087–98.
[19] Liu K, Zhang Y, Cao H, Liu H, Geng Y, Yuan W, et al. Programmable reversible shape transformation of hydrogels based on transient structural anisotropy. Adv Mater 2020;32(28):2001693.
[20] Ma C, Li T, Zhao Q, Yang X, Wu J, Luo Y, et al. Supramolecular lego assembly towards three-dimensional multi-responsive hydrogels. Adv Mater 2014;26(32): 5665–9.
[21] Wang H, Zhu CN, Zeng H, Ji X, Xie T, Yan X, et al. Reversible ion-conducting switch in a novel single-ion supramolecular hydrogel enabled by photoresponsive Host–Guest molecular recognition. Adv Mater 2019;31(12):1807328.
[22] He Q, Wang Z, Wang Y, Minori A, Tolley Michael T, Cai S. Electrically controlled liquid crystal elastomer–based soft tubular actuator with multimodal actuation. Sci Adv 2019;5(10):eaax5746.
[23] Chen S, Cao Y, Sarparast M, Yuan H, Dong L, Tan X, et al. Soft crawling robots: design, actuation, and locomotion. Adv Mater Technol 2020;5(2):1900837.
[24] Ware TH, Biggins JS, Shick AF, Warner M, White TJ. Localized soft elasticity in liquid crystal elastomers. Nat Commun 2016;7(1):10781.
[25] Kularatne RS, Kim H, Boothby JM, Ware TH. Liquid crystal elastomer actuators: synthesis, alignment, and applications. J Polym Sci, Part B: Polym Phys 2017;55 (5):395–411.
[26] Wang Y, Dang A, Zhang Z, Yin R, Gao Y, Feng L, et al. Repeatable and reprogrammable shape morphing from photoresponsive gold nanorod/liquid crystal elastomers. Adv Mater 2020;32(46):2004270.
[27] Torras N, Zinoviev KE, Marshall JE, Terentjev EM, Esteve J. Bending kinetics of a photo-actuating nematic elastomer cantilever. Appl Phys Lett 2011;99(25): 254102.
[28] Wang Y, Liu J, Yang S. Multi-functional liquid crystal elastomer composites. Appl Phys Rev 2022;9(1):011301.
[29] Wu Z, Cheng P, Zhao W, Fang J, Xu T, Chen D. Allyl sulfide-based visible light-induced dynamically reshaped liquid crystalline elastomer/SWCNT nanocomposites capable of multimode NIR photomechanical actuations. New J Chem 2020;44(26):10902–10.
[30] Montazami R, Spillmann CM, Naciri J, Ratna BR. Enhanced thermomechanical properties of a nematic liquid crystal elastomer doped with gold nanoparticles. Sens Actuators, A A 2012;178:175–8.
[31] Ambulo CP, Ford MJ, Searles K, Majidi C, Ware TH. 4D-Printable liquid metal–liquid crystal elastomer composites. ACS Appl Mater Interfaces 2021;13 (11):12805–13.
[32] Qin B, Yang W, Xu J, Wang X, Li X, Li C, et al. Photo-actuation of liquid crystalline elastomer materials doped with visible absorber dyes under quasi-daylight. Polymers 2020;12(1).
[33] Yang L, Setyowati K, Li A, Gong S, Chen J. Reversible infrared actuation of carbon nanotube–liquid crystalline elastomer nanocomposites. Adv Mater 2008;20(12): 2271–5.
[34] Ceamanos L, Kahveci Z, López-Valdeolivas M, Liu D, Broer DJ, Sánchez-Somolinos C. Four-dimensional printed liquid crystalline elastomer actuators with fast photoinduced mechanical response toward light-driven robotic functions. ACS Appl Mater Interfaces 2020;12(39):44195–204.
[35] Liu X, Wei R, Hoang PT, Wang X, Liu T, Keller P. Reversible and rapid laser actuation of liquid crystalline elastomer micropillars with inclusion of gold nanoparticles. Adv Funct Mater 2015;25(20):3022–32.
[36] Wu Z, Liu L, Cheng P, Fang J, Xu T, Chen D. Reusable gold nanorod/liquid crystalline elastomer (GNR/LCE) composite films with UV-triggered dynamic crosslinks capable of micropatterning and NIR actuation. J Mater Chem C 2019;7 (45):14245–54.
[37] Yang H, Liu J-J, Wang Z-F, Guo L-X, Keller P, Lin B-P, et al. Near-infrared-responsive gold nanorod/liquid crystalline elastomer composites prepared by sequential thiol-click chemistry. Chem Commun 2015;51(60):12126–9.
[38] Li Y, Yu H, Yu K, Guo X, Wang X. Reconfigurable three-dimensional mesotructures of spatially programmed liquid crystal elastomers and their ferromagnetic composites. Adv Funct Mater 2021;31(23):2100338.

[39] Yu L, Shahsavan H, Rivers G, Zhang C, Si P, Zhao B. Programmable 3D shape changes in liquid crystal polymer networks of uniaxial orientation. Adv Funct Mater 2018;28(37):1802809.
[40] Saed MO, Torbati AH, Nair DP, Yakacki CM. Synthesis of programmable main-chain liquid-crystalline elastomers using a two-stage thiol-acrylate reaction. JoVE 2016;107:e53546.
[41] Kim H, Zhu B, Chen H, Adetiba O, Agrawal A, Ajayan P, et al. Preparation of monodomain liquid crystal elastomers and liquid crystal elastomer nanocomposites. JoVE 2016;108:e53688.
[42] Kotikian A, McMahan C, Davidson Emily C, Muhammad Jalilah M, Weeks Robert D, Daraio C, et al. Untethered soft robotic matter with passive control of shape morphing and propulsion. Sci Rob 2019;4(33):eaax7044.
[43] Zhang M, Cao MS, Shu JC, et al. Electromagnetic absorber converting radiation for multifunction. Mater Sci Eng R Rep 2021;145:100627.
[44] Ornaghi Jr HL, Bolner AS, Fiorio R, et al. Mechanical and dynamic mechanical analysis of hybrid composites molded by resin transfer molding. J Appl Polym Sci 2010;118(2):887–96.
[45] Poletto M, Zeni M, Zattera AJ. Dynamic mechanical analysis of recycled polystyrene composites reinforced with wood flour. J Appl Polym Sci 2012;125(2):935–42.
[46] Leslie FM. Continuum theory for nematic liquid crystals. Continuum Mech Therm 1992;4:167–75.
[47] Agostiniani V, DeSimone A. Rigorous derivation of active plate models for thin sheets of nematic elastomers. Math Mech Solid 2020;25(10):1804–30.
[48] Brighenti R, McMahan CG, Cosma MP, et al. A micromechanical-based model of stimulus responsive liquid crystal elastomers. Int J Solid Struct 2021;219:92–105.
[49] Ericksen JL. Conservation laws for liquid crystals. Trans Soc Rheol 1961;5(1):23–34.
[50] Leslie FM. Some constitutive equations for liquid crystals. Arch Ration Mech Anal 1968;28:265–83.
[51] Cosma MP, Brighenti R. Controlled morphing of architected liquid crystal elastomer elements: modeling and simulations. Mech Res Commun 2022;121:103858.
[52] Biggins JS, Warner M, Bhattacharya K. Elasticity of polydomain liquid crystal elastomers. J Mech Phys Solid 2012;60(4):573–90.
[53] Agostiniani V, DeSimone A. Rigorous derivation of active plate models for thin sheets of nematic elastomers. Math Mech Solid 2020;25(10):1804–30.